Polymeric perfluoropentane nanoemulsions are a versatile platform for ultrasonic drug uncaging

Zhong, Q[†1], Yoon BC[†1], Aryal MR[1], Wang JB[1], Airan RD[1*]

1. Department of Radiology, Stanford University, Stanford, CA

† These authors contributed equally to this work.

* To whom correspondence should be addressed:
Raag Airan MD PhD
Department of Radiology, Division of Neuroradiology
Stanford University
300 Pasteur Drive, Grant Rm. S043
Stanford, CA 94305
Office: 650-724-1190
Fax: 650-736-6767
E-mail: rairan@stanford.edu

Abstract

The holy grail of drug delivery nanotechnology is the ability to target the right drug to the right part of the body at the right time. Here, we demonstrate that polymeric perfluoropentane nanoemulsions are a generalized platform for targeted drug delivery with high potential for clinical translation. We delineate a production protocol optimized for nanoparticle size, monodispersity, drug loading, and stability, and hew to clinical production standards. We confirm that varied drugs may be effectively uncaged with ultrasound using this nanoparticle system, with drug loading increasing with hydrophobicity. Finally, we exhibit the *in vivo* efficacy of this system in two organ systems: we enable targeted modulation of brain activity with anesthetic uncaging and we locally control cardiovascular function with vasodilator uncaging. This work establishes the power of polymeric perfluoropentane nanoemulsions as a clinically-translatable platform for noninvasive ultrasonic drug uncaging for myriad targets in the brain and body.

Drug delivery nanotechnologies aim to deliver a drug cargo to only the targeted organ at the appropriate time. Ultrasound-mediated drug delivery has gained much attention recently with the availability of clinical focused ultrasound systems that may sonicate any region of the body with millimeter spatial resolution[1]. These technologies may use nano- or micro-scale drug carriers that release drug after ultrasound raises the *in situ* temperature[2], activates a 'sonosensitizer'[3], or raises the tissue intensity/pressure[4] to beyond a certain threshold. While high-intensity continuous wave ultrasound may be difficult to achieve stably in certain regions of the body[5], the intensity/pressure-uncaged systems usually necessitate only short bursts of ultrasound that are more straightforward to implement *in situ*. Recently, we reported a prototype polymeric perfluoropentane nanoemulsion that would locally uncage the anesthetic propofol in the brain with short bursts of focused ultrasound (FUS), thereby enabling noninvasive pharmacologic neuromodulation[6,7]. These nanoparticles are composed of a nanoscale droplet of the high-vapor pressure liquid perfluoropentane (PFP), with drug bound by an emulsifying amphiphilic diblock-copolymer. Our model is that the drug is bound by the hydrophobic polymer block, which sits between the hydrophilic block externally and the core perfluorocarbon internally, with the external hydrophilic block insulating the drug from exposure to the medium. Upon exposure to focused ultrasound of a sufficient peak negative pressure, the core PFP of these particles expands, thinning the emulsifying polymer layer, which exposes the drug to the medium, allowing drug release (Fig. 1a)[4,6]. Past work with similar nanoparticles has suggested uses for imaging[8], oxygen delivery for ischemia[9], micro-embolization[10], thermal ablation[11–13], blood-brain barrier opening[14], and most pertinently as potential drug delivery vehicles[4]. Proofs-of-principle have been described for how this system could be used for delivering chemotherapeutics[15–17] and propofol[6]. In principle, these nanoparticles should allow encapsulation of any small molecule that is hydrophobic and therefore

able to be stably bound by the internal hydrophobic polymer block. However, to date, the range of drug and polymer characteristics that allow encapsulation into these nanoparticles has yet to be systematically described. Additionally, clinical translation demands manufacturing methods that are practically feasible, scalable, compatible with current good manufacturing practices (cGMP), and that produce particles that are sufficiently stable for a variety of uses and for storage. Furthermore, an explicit demonstration of the *in vivo* efficacy of this system in different regions of the body and on different organ systems is needed. Here, we satisfy each of these unmet needs by explicitly demonstrating the versatility of this platform for ultrasonic uncaging of a variety of drugs, with methods that enable clinical translation.

Results

Moving towards practical clinical application

To enable eventual *in vivo* and clinical applications, we first adapted our nanoparticle production methods for cGMP compatibility and scalability (Fig. 1a). We targeted a median Z-average diameter of 400-450 nm, calculated so that during uncaging the nanoparticles would be at most half of a capillary diameter, given prior theory and evidence that similar particles increase their diameter up to a maximum of 5-6 fold during uncaging[18]. We also targeted a median polydispersity index (PDI) of <0.1, to ensure monodispersity of each batch. We noted that the PFP content in the reaction significantly affected the particle size, drug loading, and monodispersity (Fig. S2), and empirically determined that a 2 μl:1 mg ratio of PFP to polymer most reliably met our target size and PDI. To generate the nanoparticles, the emulsifying polymer and drug were dissolved in tetrahydrofuran (THF), and then sterile phosphate-buffered saline (PBS) was added. The THF was evaporated to completion, leaving drug-loaded polymeric micelles in saline suspension. Then, PFP

was added and the mixture was sonicated in a bath sonicator until the PFP was visibly completely emulsified. Following three cycles of centrifugation and resuspension to remove free drug, polymer, and micelles, the nanoparticles were filtered twice through a membrane extruder to produce the final suspension. Notably, the shift from immersion sonication, as used previously[6], to bath sonication and membrane extrusion substantially reduced the free drug fraction (Fig. 1b). Dynamic light scattering confirmed that our current methods produced monodisperse peaks of nanoscale material (Fig. S1).

In prior formulations, the particle size, free drug fraction, and polydispersity all increased substantially over the course of hours with incubation on ice or at room temperature[6], and the particles were too unstable to permit a freeze-thaw cycle. This is in keeping with prior experience with similar particles[15]. To address this significant practical limitation, we used cryoprotectants to enable frozen storage of the particles. While the addition of minimal (2.25% w/v) glycerin to the particles had no substantial effect on the physicochemical characteristics and drug loading of the particles (Figs. 1c, S3a,b), it allowed for improved particle stability in terms of physicochemical characteristics in the post-thaw time period (Figs. 1d, S3c,d) and permitted long-term frozen storage of the particles (Figs. 1e, S3e,f) with stability across multiple freeze-thaw cycles (Fig. S4). This formulation also showed low batch-to-batch variability with no change of physicochemical characteristics across varied particle concentrations (Fig. S3g-i, indexed by the encapsulated drug concentration). In our current protocol, there is a minimal slow increase of the free drug fraction during room temperature incubation, rising from ~4% of the initial drug load when fresh to ~8% after 3 hours post-thaw at room temperature (Fig. 1d). In practice, we make use of the particles within 3 hours of thawing.

To determine the efficacy of the particles for ultrasonic drug uncaging *in vitro*, we loaded the particles into thin-walled plastic (PCR) tubes and then added a layer of organic solvent on top that was immiscible with and of lower density than water (Fig. 1f). Following focused sonication of the aqueous nanoparticle suspension, the organic layer was collected, and the UV fluorescence of this fraction was measured to indicate the amount of drug release. Indeed, there was robust FUS-induced drug release seen with a dose-response relationship with the applied *in situ* peak pressure, and no change of this efficacy between fresh and frozen/thawed nanoparticles, irrespective of the length of time that the particles were frozen (Fig. 1g). With 650 kHz sonication, a drug release sonication pressure threshold of 0.8 MPa was estimated (Figs. 1g, 3d), with an estimated threshold of 1.2 MPa at 1.5 MHz (Fig. 2d). Drug release also increased with sonication burst length, with minimal or no appreciable release below 10 ms and saturation of the effect above 50 ms.

To determine the effect of the encapsulating diblock-copolymer on drug loading and release efficacy, we varied the hydrophobic block of the polymer between the common drug delivery polymers of poly-ε -caprolactone (PCL), poly-L-lactic acid (PLLA), and poly-lactic-co-glycolic acid (PLGA). The molecular weight of these blocks was varied between 2 kDa and 5 kDa. The hydrophilic block of poly-ethylene glycol (PEG; mol. wt. 2 kDa) was kept constant. PLLA particles, particularly with a block molecular weight of 5 kDa, showed increased size and polydispersity, and in many cases developed a precipitate during production (biasing the drug loading estimates), indicating that this polymer was not suitable for these applications (Fig. 2). There was minimal difference between PCL and PLGA in terms of the resultant particle physicochemical characteristics and drug loading. Larger hydrophobic blocks yielded greater drug loading (Fig. 2c), with approximately double the drug loading with 5 kDa hydrophobic block sizes compared to 2 kDa. There was minimal difference among the particles in terms of *in vitro*

ultrasonic drug uncaging efficacy (Fig. 2d), with larger hydrophobic blocks trending towards minimally decreased percent uncaging. Given the substantially improved drug loading of 5 kDa vs. 2 kDa hydrophobic blocks relative to this minimally decreased percent uncaging, and the greater reported experience of safety and efficacy in clinical drug delivery applications with PLGA[19] compared to PCL, we chose PEG(2 kDa)-PLGA(5 kDa) as the emulsifying polymer of the nanoemulsions for subsequent experiments.

A generalized platform for drug delivery

To realize the promise of this system as a platform for targeted delivery of a wide variety of drugs, and to estimate the drug features that most enable encapsulation into polymeric perfluoropentane nanoemulsions, we varied the drug across seven molecules: two vasoactive agents (calcium channel antagonists verapamil and nicardipine), three anesthetics (propofol, ketamine, and dexmedetomidine), and two chemotherapeutics (doxorubicin and cisplatin). There was minimal difference of the encapsulated drug on the particle physicochemical properties (Figs. 3a,b). Instead, there was a strong positive relationship noted between the drug LogP (a measure of hydrophobicity) and the drug loading (Fig. 3c), with essentially no loading of the hydrophilic compound cisplatin. Interestingly, while there were minimal differences of *in vitro* ultrasonic drug uncaging efficacy across the different drugs (Fig. 3d), there was a reverse trend compared to drug loading in that doxorubicin (LogP=1.3) had the greatest drug release versus applied pressure, compared to verapamil or nicardipine (LogP=3.8). These results establish the generalizability of this system for ultrasonic uncaging of hydrophobic drugs.

In vivo nanoparticle characteristics

To determine the clearance kinetics, biodistribution, and biocompatibility of the particles in rats, in addition to the indicated drug, the particles were doped with a dye whose infrared fluorescence is quantitative *in vivo* and in blood samples, and which in its unincorporated free form clears from the blood pool within ~5 min. For this analysis, we chose among the drugs with substantial loading (Fig. 2), drugs with high (nicardipine), intermediate (propofol), and low (doxorubicin) drug loading. To assess particle clearance kinetics, the fluorescence was quantified for whole blood and plasma samples collected at several time points over hours. The difference between the whole-blood and plasma sample fluorescence indicated the nanoparticle blood concentration. The plasma fluorescence indicated the rate of generation of drug-loaded micelles as the volatile PFP diffuses out of the nanoparticle core, as well as the potential elution of free dye. There was no substantial effect of the encapsulated drug on particle kinetics or biodistribution (Figs. 4). For each drug, the particle blood pool concentration followed a dual exponential clearance profile, with half-lives of 10-12 min for a redistribution phase and 77-97 min for an elimination phase (Fig. S5; Tables S1-2). Based on this profile, a bolus plus infusion protocol was determined to yield a steady blood particle concentration to enable prolonged usage. Indeed, with this bolus plus infusion protocol, a steady blood pool particle concentration was seen for over 40 min, with a similar elimination profile to bolus alone following the halt of infusion (Fig. 4b). Independent of the loaded drug, the particles showed uptake at 24 h primarily in the liver, followed by spleen and lung, with minimal uptake in kidney and heart, and notably no binding to the brain (Fig. 4e-f). In our experiments, >80 rats have received the current formulation of these particles, with some receiving up to nine doses over several weeks, and none have shown visible evidence of toxicity due to particle administration or uncaging. Indeed, no negative change was seen in animal body weight across two weeks of multiple nanoparticle administrations (Fig. 4g). These results indicate that,

independent of the choice of loaded drug, these nanoparticles are well tolerated and have clinically practical clearance kinetics to enable acute ultrasonic drug uncaging therapies.

Efficacious ultrasonic drug uncaging in the nervous system

Following these optimizations, we next sought to confirm that these particles retained a similar efficacy *in vivo* as was shown in our prior proof-of-principle study[6]. We assayed the response of visual evoked potentials (VEPs), an electrophysiological assay of brain function, to ultrasonic propofol uncaging in rat primary visual cortex (V1). Light flashes (10ms @1 Hz) were administered to one eye of a rat (Fig. 5a). A 650 kHz focused ultrasound transducer was coupled to target the contralateral V1. Electrophysiological potentials in response to the light flashes were recorded by a skull electrode placed near midline over the occipital cortex, with a reference electrode in the rostral frontal bone. Each rat underwent the same protocol in which, after the recorded potentials reached a threshold signal amplitude (N1P1 amplitude >60 μV), FUS was applied (60 x 50 ms pulses, 1 Hz pulse repetition frequency, 1.2 MPa estimated peak *in situ* pressure) to V1 without nanoparticles in circulation, while recording VEPs. Then, while recording VEPs, propofol-loaded phase-change nanoparticles were administered intravenously as a bolus of an encapsulated propofol dose of 1 mg/kg body weight. Then, after waiting at least 10 min from nanoparticle administration to allow redistribution (Fig. 4a), the same FUS protocol was applied to V1. A substantial reduction in the N1P1 VEP amplitude was noted with sonication with nanoparticles in circulation (Fig. 5b-d), indicating an effective anesthesia induced by ultrasonic propofol uncaging. Notably, FUS alone had no similar effect. Nanoparticle administration itself did not yield such a decrease, and instead induced a slight increase in VEP amplitude, presumably due to a net stimulatory effect of bolus fluid administration. Further, the anesthetic effect of

ultrasonic propofol uncaging was limited by the time period of ultrasound application, with anesthesia onset commencing with FUS onset, and recovery commencing with FUS offset (Fig. 5c). In our prior work, we were able to knock out seizure activity in rats[6], as a proof-of-principle that this system is effective for ultrasonic drug uncaging to attenuate pathologic brain activity. These results confirm that this system can be used for effective ultrasonic propofol uncaging to reversibly knock out physiological brain activity.

Efficacious ultrasonic contrast enhancement and drug uncaging in the cardiovascular system

We next noted that the acoustic impedance of PFP at 37 °C is 0.67 MRayl[20], and that of blood or soft tissue is typically 1.6-1.7 MRayl[21]. This difference in acoustic impedance suggests that polymeric PFP nanoemulsions should be echogenic in the body, and therefore could serve as ultrasound contrast agents. Indeed, both *in vitro* (Fig. 6a) and *in vivo* (Fig. 6b), we see that the presence of PFP nanoparticles substantially increased power Doppler ultrasound signals, allowing for more sensitive vascular imaging.

Next, we noted that in the ultrasonic propofol uncaging experiments (Fig. 5), the uncaged drug had the opportunity to enter into and act upon the brain parenchyma across the blood-brain barrier during the whole time it traversed the capillary bed (order of seconds[22]). We sought to assess whether ultrasonic drug uncaging could measurably affect physiological systems after uncaging in larger vessels with faster flows, where there is not as much time for the critical drug-receptor interaction. Vasodilating agents, such as nicardipine and verapamil are used clinically to relieve arterial spasm as seen with cerebral vasospasm and other conditions[23], by relaxing the smooth muscle of the vessel wall. For example, nicardipine has been shown to relax the wall of the aorta and increase its distensibility in humans[24]. While effective, these agents have undesirable

side effects of generalized hypotension when given systemically, due to decreasing the systemic vascular resistance by action beyond the target vessel. This hypotension can result in end organ infarction in severe cases. In order to minimize this effect, the vasodilator must be infused via an invasive intra-arterial catheter placed within the target vessel or immediately upstream. For ultrasonic vasodilator uncaging to achieve similar effects, the vasodilator must bind the arterial smooth muscle immediately after ultrasound-induced release from the nanoparticles, given that arterial velocities are generally on the order of 0.3-0.5 m/s[25]. We therefore assessed whether ultrasonic nicardipine uncaging could yield a visible change in vessel wall compliance of the rat abdominal aorta (~7 cm in length, ~1 mm luminal diameter), indicated by the change in vessel diameter over the cardiac cycle. With ultrasonic nicardipine uncaging in the aorta upstream of an ultrasound imaging probe, a substantial difference in systolic and diastolic aortic diameters was noted compared to the pre-uncaging baseline (Fig. 6c-f; Videos S1-2). Confirming its specificity, this effect was not seen with ultrasound alone, with nanoparticle administration alone, with ultrasound applied to blank nanoparticles, or with nicardipine uncaging applied downstream ('Position 2') of the imaging probe (Fig. 6e). In fact, compared with a systemic bolus of free nicardipine that is matched in terms of the total nicardipine dose, ultrasonically uncaged nicardipine had a more potent effect on the vessel wall distensibility (Fig. 6e), even though it is likely that only a minority of the nanoparticles were exposed to the sonication field. Additionally, systemic nicardipine administration increased the aortic blood velocity, due to a decrease in systemic vascular resistance with peripheral nicardipine action (Fig. S6). Similarly, uncaging of nicardipine nanoparticles in the distal aorta increased the blood flow velocity in the aorta (Fig. S6), likely by relaxing the arterial/arteriolar smooth muscle in the lower limbs and therefore decreasing the vascular resistance seen by the lower aortic blood flow. However, importantly, this effect was

not seen with ultrasonic nicardipine uncaging in the proximal aorta, confirming that ultrasonic drug uncaging is limited to effects in the immediate region of sonication, given the length of the rat aorta (~7 cm) and the rapid speed of rat aortic flows (~0.3-0.5 m/s; Fig. S6). This confirms that ultrasonic drug uncaging yields a volume of distribution of the drug that is confined to the sonicated region, which in turn results in an effective amplification of the local drug effect. Furthermore, these results demonstrate that this localized drug-receptor binding can occur even in the presence of rapid aortic flows. Notably, the majority of this effect occurred with the first minute of sonication (Fig. 6f), confirming the rapid temporal kinetics of the bioeffects of ultrasonic drug uncaging.

3. Discussion

We have shown that polymeric PFP nanodroplets are a versatile platform for ultrasonic drug uncaging, with a ready path for clinical translation. We have described scalable production methods that are cGMP-compatible and which produce particles that are stable for both long-term frozen storage and for hours of use after thawing (Figs. 1, S1-4). We have confirmed that longer hydrophobic blocks of the emulsifying polymer yield greater drug loading, with minimal effect of the choice of polymer on drug uncaging efficacy (Fig. 2). We further explicitly demonstrate the ability of this technology to encapsulate and selectively uncage drugs that span a range of hydrophobicity, drug classes, and receptor binding profiles (Fig. 3). Indeed, the clearance kinetics and biodistribution of these nanoparticles appears to be independent of the particular drug that is encapsulated (Figs. 4, S5; Tables S1-2). Finally, we demonstrate the utility of ultrasonic drug uncaging to yield potent localized pharmacological bioeffects both in the brain (Fig. 5) and in the body (Fig. 6). Specifically, we show that ultrasonic propofol uncaging can yield a potent anesthesia

of the visual cortex with sonication (Fig. 5). We further show that these are theranostic particles as they act both as ultrasound contrast agents for vascular imaging (Fig. 6a,b) and may yield focal vessel wall relaxation with ultrasonic nicardipine uncaging that is spatially restricted to the target vessel, even in the setting of rapid aortic flows (Figs. 6c-f, S6; Videos S1-2).

There are myriad potential applications for ultrasonic drug uncaging. In the brain, focal uncaging of neuromodulatory agents could allow pharmacological adjuncts to psychiatric therapy sessions that are tailored to the particular neural circuit pathophysiology for a given patient. This technology could also allow pharmacological mapping of neural circuits to better target more permanent interventions such as surgical resection, ablation, or deep-brain stimulation. Additionally, the treatment of vessel spasm disorders, such as the cerebral vasospasm that unfortunately accompanies many cases of subarachnoid hemorrhage[23], is difficult given that the agents that best relieve the spasm also act systemically as potent anti-hypertensives. The improved vessel imaging with these particles (Fig. 6a,b) could improve the diagnosis of vasospasm, and noninvasive local relaxation of the walls of the affected vessels, as modeled in Fig. 6c-f, would be enormously beneficial, especially without concomitant loss of systemic vascular resistance and therefore systemic hypotension. Finally, many chemotherapeutics are known to be effective for treatment of a given tumor yet cannot be administered in effective doses systemically due to intolerable side effects in the rest of the body. Ultrasonic chemotherapeutic uncaging within the tumor and its immediate margin would therefore be of great utility.

Future work with this technology will move ultrasonic drug uncaging to clinical practice, first by validating this approach in large animal models, and then by beginning first-in-human trials to establish the safety and drug uncaging efficacy of this technique. Importantly, the constituent components of these nanoparticles – namely the drugs under consideration, PEG,

PLGA[19], and PFP[26] droplets – have each been used in clinical populations with excellent safety profiles, lowering the barrier to translation for these nanoparticles. Additional future work will focus on expanding this technology to include encapsulation of hydrophilic small molecules, as well as larger macromolecules like peptides, antibodies, and nucleic acids. Given their potential for clinical translation, their ability to uncage a variety of important drugs, and the potent local pharmacological bioeffects they can induce, polymeric perfluoropentane nanoemulsions are poised to have enormous impact both for clinical care as well as our scientific understanding of how pharmaceuticals mediate their effects.

Figures

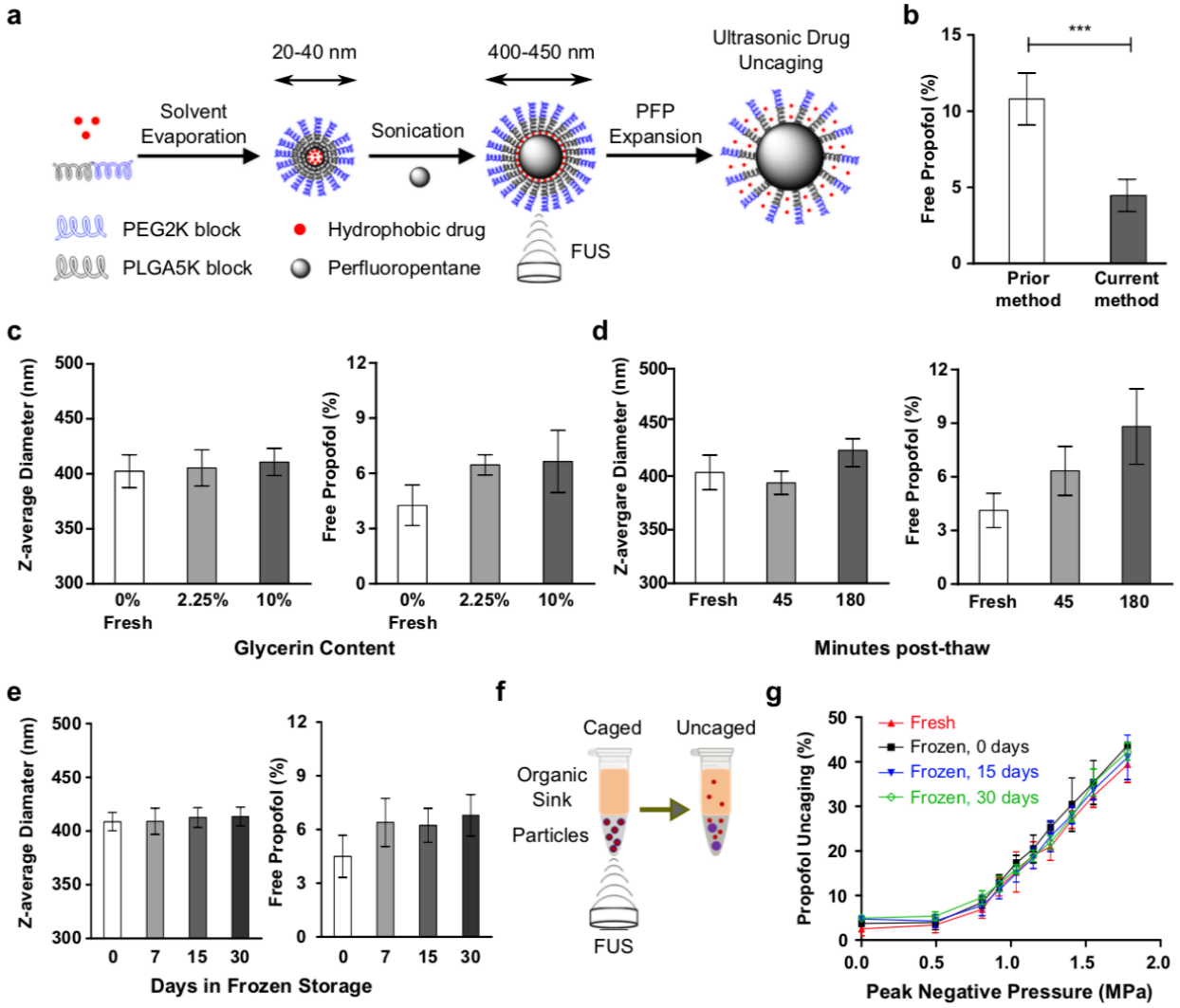

Figure 1 | Optimized nanoparticle production for stability and efficacy *in vitro*. a. Schematic of nanoparticle production and ultrasonic drug uncaging. **b**. Free propofol content is reduced with the current optimized protocol versus the prior[6]. **c-e**. Glycerin serves as a cryoprotectant to improve nanoparticle stability through frozen storage and thawing. **f**. Experimental schematic to assay ultrasonic drug uncaging efficacy *in vitro*. **g**. Intact ultrasonic drug uncaging efficacy *in vitro* (650 kHz sonication, 60 x 50 ms pulses at 1 Hz pulse repetition frequency) for frozen & thawed nanoparticles compared to fresh. Mean +/- S.D. are presented for groups of N=3. ***: $p < 0.001$ by two-tailed t-test.

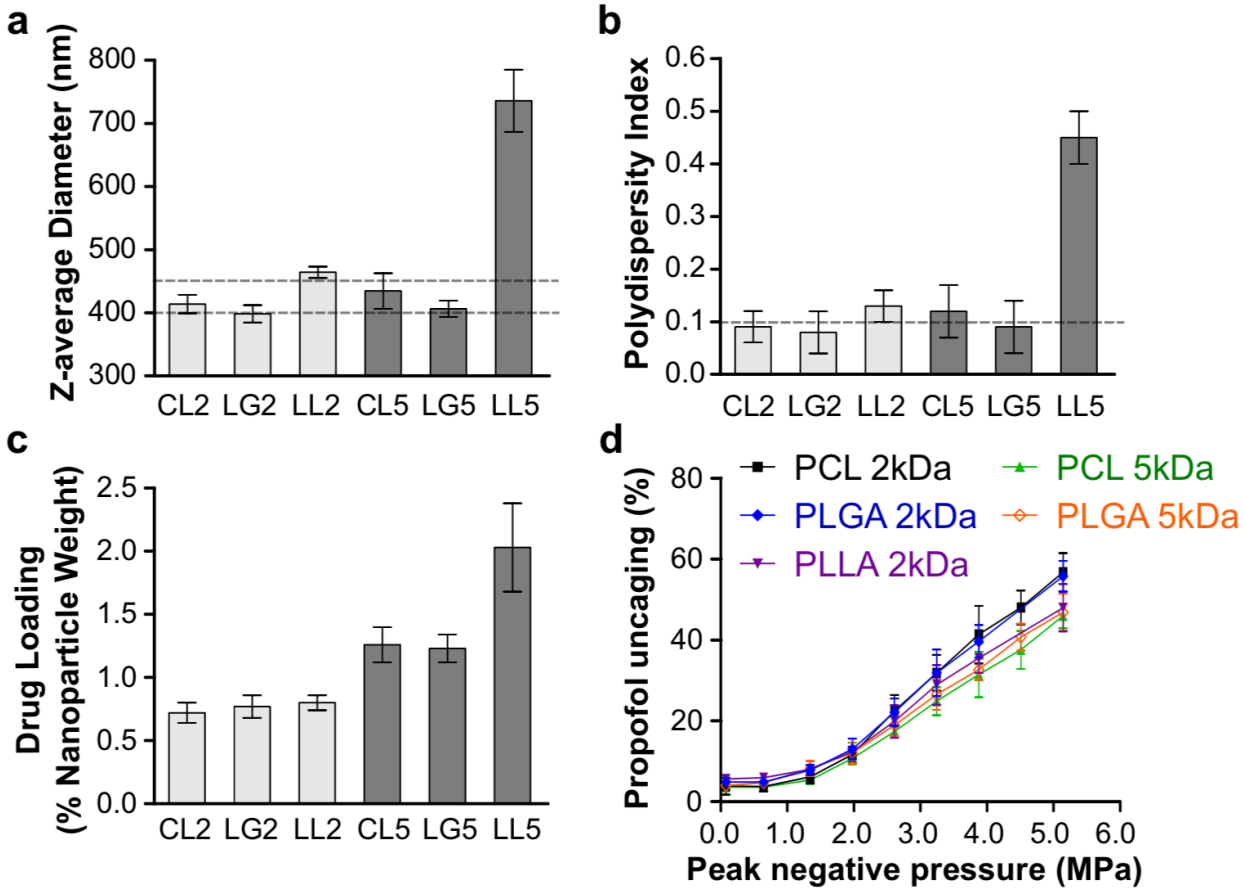

Figure 2 | Optimization of polymer choice for drug-loaded perfluoropentane nanoemulsions. Diblock-copolymers were tested consisting of a hydrophilic block of PEG (2 kDa) and a choice of hydrophobic block among: PCL (2 kDa, CL2 or 5 kDa, CL5), PLGA (2 kDa, LG2 or 5 kDa, LG5), or PLLA (2 kDa, LL2 or 5 kDa, LL5) **a**, Z-average diameter (dashed lines at the target values of 400-450 nm), **b**, polydispersity index (dashed line at target value of 0.1), **c**, propofol drug loading, and **d**, ultrasonic propofol uncaging *in vitro* (1.5 MHz sonication, 60 x 50 ms pulses at 1 Hz pulse repetition frequency) was quantified. Mean +/- S.D. are presented for groups of N=3.

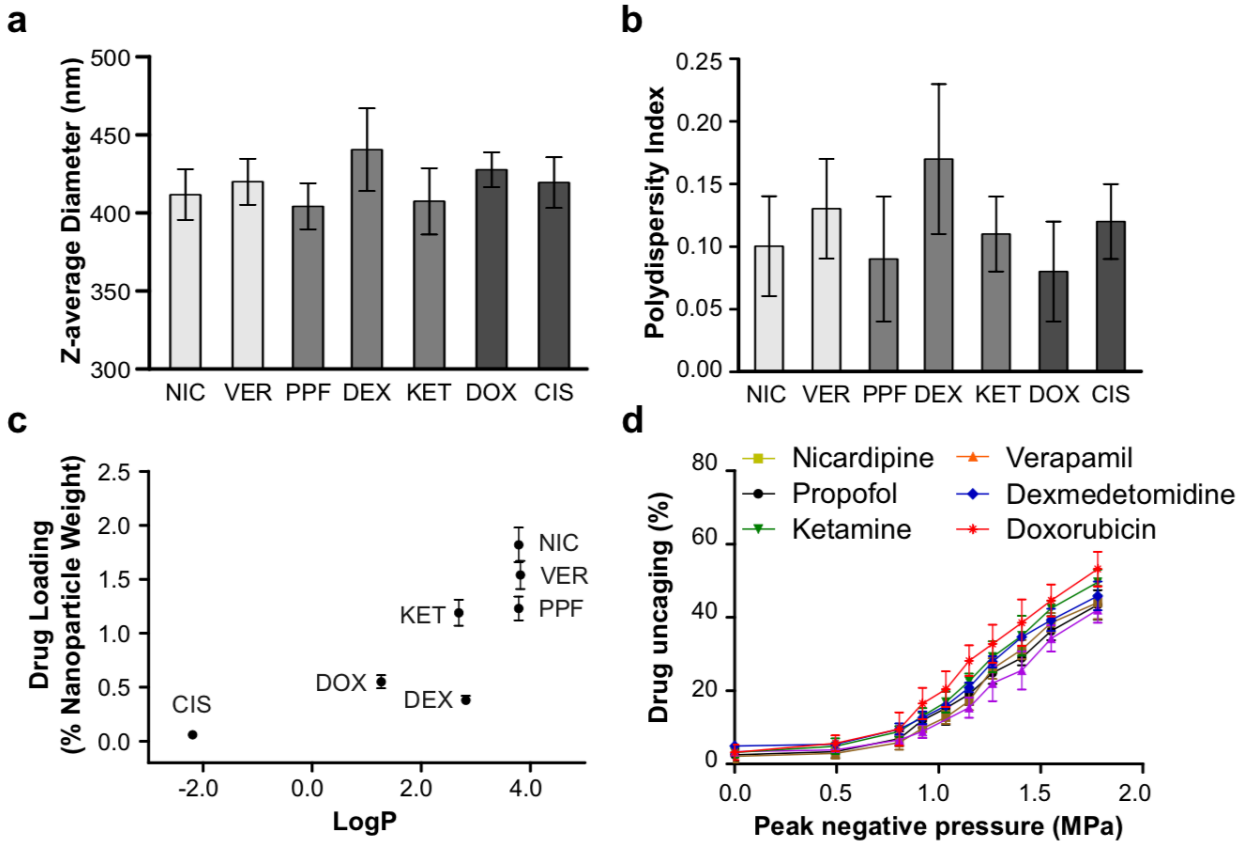

Figure 3 | Polymeric perfluoropentane nanoemulsions are a platform for ultrasonic uncaging of hydrophobic drugs. **a**, Z-average diameter, **b**, polydispersity index, **c**, drug loading, and **d,** ultrasonic drug uncaging *in vitro* (650 kHz sonication, 60 x 50 ms pulses at 1 Hz pulse repetition frequency) of PEG(2 kDa)-PLGA(5 kDa) perfluoropentane nanoemulsions loaded with propofol (PPF), nicardipine (NIC), verapamil (VER), dexmedetomidine (DEX), ketamine (KET), doxorubicin (DOX), or cisplatin (CIS). Mean +/- S.D. are presented for groups of N=3. Cisplatin-loaded nanoparticles were not tested for *in vitro* uncaging due to extremely low drug loading. In the bar charts, drugs of a similar class (vasodilators, anesthetics, chemotherapeutics) are grouped.

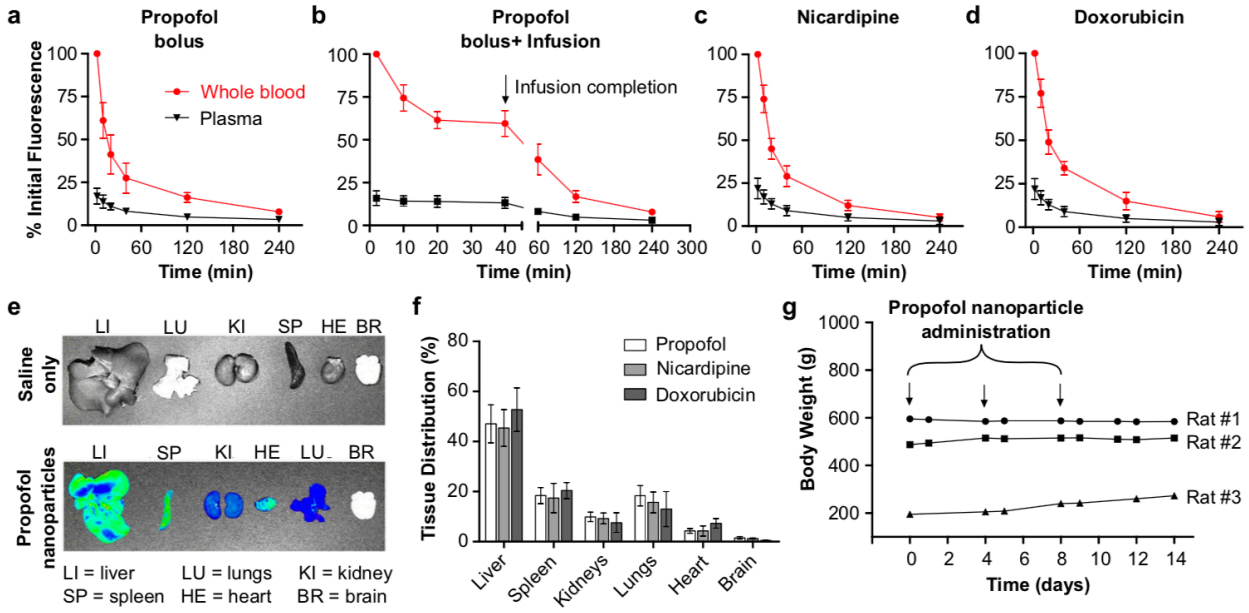

Figure 4 | Particle clearance kinetics, biodistribution, and biotolerance. Particle kinetics after intravenous administration of **a**, propofol-loaded nanoparticles (bolus of 1 mg/kg encapsulated propofol), **b**, propofol-loaded nanoparticles as an i.v. infusion (bolus of 1 mg/kg + infusion of 1.5 mg/kg/hr encapsulated propofol), **c**, nicardipine-loaded nanoparticles (bolus of 1 mg/kg encapsulated nicardipine), and **d**, doxorubicin-loaded nanoparticles (bolus of 1 mg/kg encapsulated doxorubicin). **e,** Sample images of IR dye fluorescence in organs harvested 24 h after saline (top) and nanoparticle (bottom) administration to rats. **f**, Tissue distribution of propofol, nicardipine, or doxorubicin-loaded nanoparticles 24 h after i.v bolus (1 mg/kg encapsulated drug). **g**, Body weight of rats administered 3 boluses of propofol-loaded nanoparticles over 8 days. On Day 0, Rat #1: 15 weeks old and body weight 595 g; Rat#2: 11 weeks old and body weight 457 g; Rat#3: 5 weeks old and body weight 195 g. Mean +/- S.D. are presented for groups of N=3.

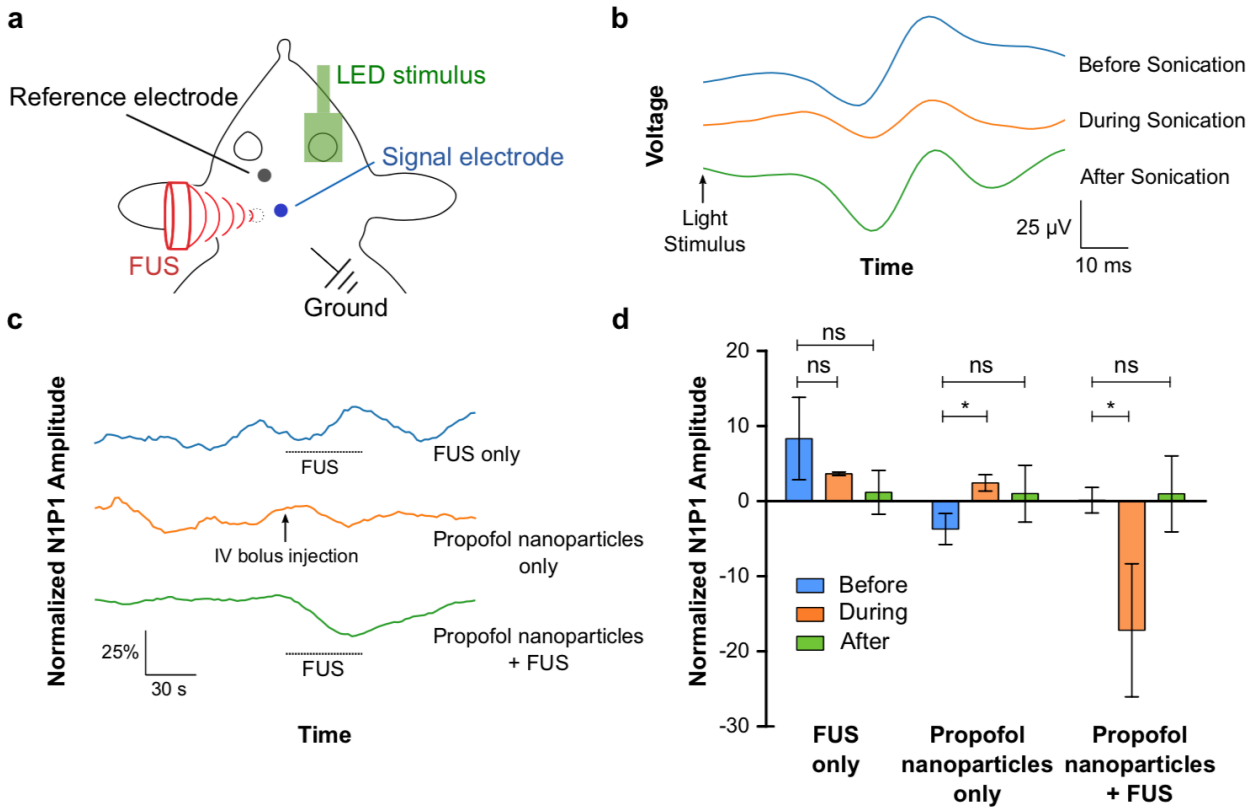

Figure 5 | Ultrasonic propofol uncaging reversibly anesthetizes the visual cortex. **a**, Experimental schematic for measuring rat visual evoked potentials (VEPs). **b**, Averaged VEP waveforms before, during, and after sonication (650 kHz, 60 x 50 ms pulses at 1 Hz pulse repetition frequency, 1.2 MPa est. peak *in situ* pressure) in animals with propofol-loaded nanoparticles in circulation. **c**, VEP N1P1 amplitude across time. **d**, Average N1P1 amplitude during a 60 s epoch before, during, or after sonication (FUS only and Propofol nanoparticles + FUS groups) or nanoparticle administration (Propofol nanoparticles only group). Mean +/- S.D. are presented for groups of N=3. ns: not significant, *: $p < 0.05$ by two-tailed t-test.

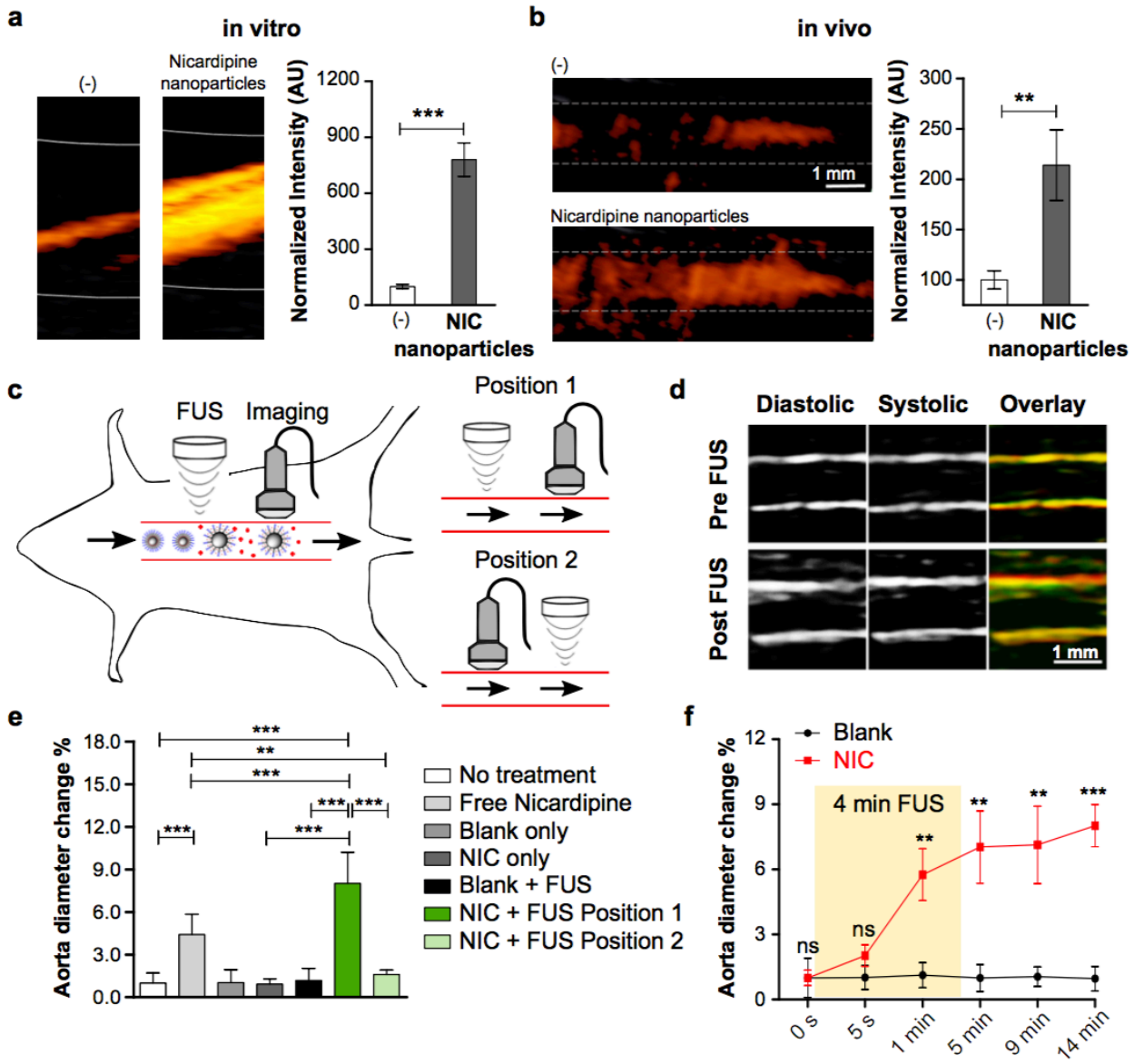

Figure 6 | Ultrasonic nicardipine uncaging locally increases vessel compliance. Nicardipine-loaded nanoparticles increase power Doppler ultrasound signal **a**, *in vitro* and **b**, *in vivo*. **c**, Experimental schematic to test if ultrasonic nicardipine uncaging increases rat aortic wall compliance. Uncaging is applied to the aorta either upstream (Position 1) or downstream (Position 2) of imaging. **d**, Ultrasound images of the rat abdominal aorta during systole and diastole, before and after ultrasonic nicardipine uncaging (650 kHz, 240 x 50 ms pulses at 1 Hz pulse repetition frequency, 1.5 MPa est. peak *in situ* pressure); Overlay: green = diastolic, red = systolic, yellow = green/red overlap. Averaged rat abdominal aortic diameter at **e,** 14 min after uncaging or **f**, across time, normalized by the initial (0 s) values. FUS = focused ultrasound application, NIC = nicardipine-loaded nanoparticles. Free nicardipine and NIC administered to total drug dose of 134

μg/kg i.v. Mean +/- S.D. are presented for groups of N=3 (**a, b**) and N=5-6 (**e, f**). ns: not significant, **: $p < 0.01$; ***: $p < 0.001$ by two-tailed Student's t-tests between the nicardipine-loaded nanoparticles and the corresponding negative conditions (**a, b**, **f**) or ANOVA and Tukey post-hoc tests (**e,** $F(6,30)=28.49$).

References

1. Kim, Y. Advances in MR image-guided high-intensity focused ultrasound therapy. *Int. J. Hyperth.* **31,** 225–232 (2015).
2. Hossann, M., Kneidl, B., Peller, M., Lindner, L. & Winter, G. Thermosensitive liposomal drug delivery systems: state of the art review. *Int. J. Nanomedicine* **9,** 4387 (2014).
3. Rwei, A. Y. *et al.* Ultrasound-triggered local anaesthesia. *Nat. Biomed. Eng.* **1,** 644–653 (2017).
4. Rapoport, N. Drug-Loaded Perfluorocarbon Nanodroplets for Ultrasound-Mediated Drug Delivery. *Adv. Exp. Med. Biol.* **880,** 221–41 (2016).
5. Dou, Y., Hynynen, K. & Allen, C. To heat or not to heat: Challenges with clinical translation of thermosensitive liposomes. *J. Control. Release* **249,** 63–73 (2017).
6. Airan, R. D. *et al.* Noninvasive Targeted Transcranial Neuromodulation via Focused Ultrasound Gated Drug Release from Nanoemulsions. *Nano Lett.* **17,** 652–659 (2017).
7. Airan, R. Neuromodulation with nanoparticles. *Science* **357,** 465 (2017).
8. Dayton, P. A. *et al.* Application of ultrasound to selectively localize nanodroplets for targeted imaging and therapy. *Mol. Imaging* **5,** 160–74 (2006).
9. Woods, S. D. *et al.* Progress in Dodecafluoropentane Emulsion as a Neuroprotective Agent in a Rabbit Stroke Model. *Mol. Neurobiol.* **48,** 363–367 (2013).
10. Zhang, M. *et al.* Initial Investigation of Acoustic Droplet Vaporization for Occlusion in Canine Kidney. *Ultrasound Med. Biol.* **36,** 1691–1703 (2010).
11. Zhang, M. *et al.* Acoustic Droplet Vaporization for Enhancement of Thermal Ablation by High Intensity Focused Ultrasound. *Acad. Radiol.* **18,** 1123–1132 (2011).
12. Kopechek, J. A., Zhang, P., Burgess, M. T. & Porter, T. M. Synthesis of phase-shift nanoemulsions with narrow size distributions for acoustic droplet vaporization and

bubble-enhanced ultrasound-mediated ablation. *J. Vis. Exp.* e4308 (2012). doi:10.3791/4308

13. Zhang, P., Kopechek, J. A. & Porter, T. M. The impact of vaporized nanoemulsions on ultrasound-mediated ablation. *J. Ther. Ultrasound 2013 11* **1,** 2 (2013).

14. Chen, C. C. *et al.* Targeted drug delivery with focused ultrasound-induced blood-brain barrier opening using acoustically-activated nanodroplets. *J. Control. Release* **172,** 795–804 (2013).

15. Rapoport, N. *et al.* Ultrasound-mediated tumor imaging and nanotherapy using drug loaded, block copolymer stabilized perfluorocarbon nanoemulsions. *J. Control. Release* **153,** 4–15 (2011).

16. Gao, Z., Kennedy, A. M., Christensen, D. A. & Rapoport, N. Y. Drug-loaded nano/microbubbles for combining ultrasonography and targeted chemotherapy. *Ultrasonics* **48,** 260–70 (2008).

17. Fabiilli, M. L. *et al.* Delivery of Chlorambucil Using an Acoustically-Triggered Perfluoropentane Emulsion. *Ultrasound Med. Biol.* **36,** 1364–1375 (2010).

18. Sheeran, P. S. & Dayton, P. A. Phase-Change Contrast Agents for Imaging and Therapy. *Curr. Pharm. Des.* **18,** 2152–2165 (2012).

19. Makadia, H. K. & Siegel, S. J. Poly Lactic-co-Glycolic Acid (PLGA) as Biodegradable Controlled Drug Delivery Carrier. *Polymers (Basel).* **3,** 1377–1397 (2011).

20. Shpak, O. *et al.* Acoustic droplet vaporization is initiated by superharmonic focusing. doi:10.1073/pnas.1312171111

21. Appendix A: Typical Acoustic Properties of Tissues. in *Basics of Biomedical Ultrasound for Engineers* 313–314 (John Wiley & Sons, Inc., 2010).

doi:10.1002/9780470561478.app1

22. Hudetz, A. G. Blood Flow in the Cerebral Capillary Network: A Review Emphasizing Observations with Intravital Microscopy. *Microcirculation* **4,** 233–252 (1997).

23. Kumar, G., Shahripour, R. B. & Harrigan, M. R. Vasospasm on transcranial Doppler is predictive of delayed cerebral ischemia in aneurysmal subarachnoid hemorrhage: a systematic review and meta-analysis. *J. Neurosurg*. **124,** 1257–1264 (2016).

24. Honda, T. *et al*. Effect of antihypertensive therapy on aortic distensibility in patients with essential hypertension: comparison with trichlormethiazide, nicardipine and alacepril. *Cardiovasc. drugs Ther*. **13,** 339–46 (1999).

25. Benessiano, J., Levy, B. I. & Michel, J.-B. Instantaneous aortic blood flow measurement with range-gated doppler flowmeter in anesthetized rat. *J. Pharmacol. Methods* **14,** 99–110 (1985).

26. University of Arkansas. A Phase 1b in Patients With Acute Ischemic Stroke - Full Text View - ClinicalTrials.gov. *ClinicalTrials.gov* (2016). Available at: https://clinicaltrials.gov/ct2/show/study/NCT02963376. (Accessed: 2nd April 2018)

Acknowledgements

This work was funded with grant support from the National Institutes of Health (BRAIN Initiative RF1 MH114252), the Stanford Center for Cancer Nanotechnology Excellence, the Foundation of the American Society for Neuroradiology, and the Wallace H. Coulter Foundation. We would also like to thank William T. Newsome, PhD and the Stanford Neurosciences Institute for additional funding support. We would like to thank Yun-Sheng Chen, PhD and Ananya Karthik for their assistance in the design and preparation of the nanoemulsions, and Marko Jakovljevic, PhD and Jeremy Dahl, PhD for access to and training on the Siemens Acuson S2000 scanner. We would like to thank Kim Butts Pauly, PhD, Jennifer Dionne, PhD, and the whole Airan Lab for helpful discussions.

Author Contributions

QZ and RDA designed the experiments. QZ performed the chemistry of nanoparticle production and physicochemical characterization. QZ performed the *in vitro* ultrasonic drug uncaging experiments, with guidance from MA. MA and JBW calibrated the focused ultrasound equipment and performed and completed analysis for the EEG ultrasonic propofol uncaging experiments. QZ and BCY performed the ultrasound imaging and ultrasonic nicardipine uncaging experiments and their analysis. QZ, BCY, and RDA prepared the figures and wrote the manuscript.

Competing Interests

Patent applications have been filed on inventions described in this manuscript (17-163 – Provisional application with Stanford University; QZ and RDA) and on related technology (PCT/US2017/033226 with Johns Hopkins University; RDA).